A switched-reluctance motor for aerospace application: design, analysis and results

M. Tursini, M. Villani, G. Fabri, L. Di Leonardo

***Abstract* -- This paper presents a five-phase switched reluctance motor designed to satisfy the requirements of flap actuators in medium size aircrafts, a real example of the More Electric Aircraft trend. In normal conditions the machine operates with two phases conducting simultaneously but it is designed to satisfy the load specifications also with one or two phases open as consequence of fault remedial strategies. A finite-element study, aiming to predict both the healthy and faulty-mode performance, is presented. The mean torque vs. current capability and the torque ripple are investigated and optimum commutation angles are evaluated in static conditions. Experimental tests on the motor prototype are included, which confirm its capability to satisfy the planned degraded modes of operation and validate the design.**

***Index Terms* — Aircraft actuator; multi-phase motor; switched-reluctance motor; design optimization; fault-tolerance; finite element analysis.**

NOMENCLATURE

B	air-gap flux density at the aligned position;
L	active motor length;
D	bore diameter;
Δ	specific electric loading;
N_{ph}	number of phases;
$N_{ph}^{'}$	number of phases conducting simultaneously;
N_s	number of stator poles;
N_r	number of rotor poles;
N_t	number of turns per phase;
η	motor efficiency;
n_s	rotor speed in rpm;
I	peak phase current;
V	peak phase voltage;
$A,...,E$	phases of the motor.

I. INTRODUCTION

Switched-Reluctance (SR) machines have a simple mechanical structure without windings and permanent magnets on the rotor: both the stator and rotor have salient poles, hence they are referred to as doubly salient machines, [1][2].

Though its origin dates back to the nineteenth century, the SR machine was ignored for a long time due to its poor performance. The developments in power electronics and converters achieved in the last decades and the use of accurate design procedures have brought to reconsider and propose this type of machine for all those applications in which robustness is a must. Several examples can be found in literature, both in variable speed drives, [3]-[7], and in power generation, [8][9].

In particular, SR motors have been considered as the engine of electromechanical actuators (EMAs) devised to replace the well established hydraulic and pneumatic actuators in More Electric Aircrafts (MEAs). Such an interest is related to the matter that SR motors enable direct exploitation of fault-tolerance criteria, [10],[12].

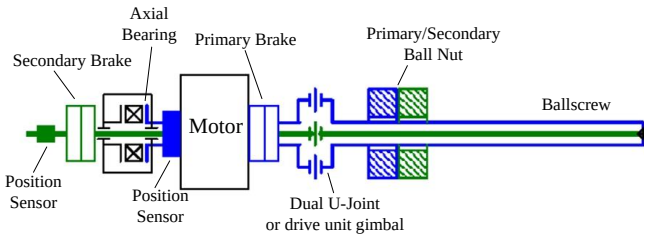

Fig. 1. Block scheme of the flap-actuator.

In fact, electrical drives for aircraft application must assure reliability levels much greater than those required in industry, and this involves specific design strategies [13].

One feasible approach aiming at including fault-tolerance in electrical drives is the one which allows to foresee redundancy and independence of the phases in their structure. The design concept is based on a modular approach whereby each phase (module) is as much as possible insulated from the others as regard to electrical, magnetic and thermal issues. As to the motor structure, such principles have the natural implementation through the use of concentrated stator windings, [14].

The SR motor represents an effective candidate for aircraft applications because of its inherent modularity and fault-tolerance. In fact, its structure is strictly based on concentrated windings and the lack of permanent magnets (PM) makes the machine behavior independent from temperature and safe as regards some important failure conditions.

Compared to PM machines, the SR motor is much more robust, easy to build, and cheaper and it has the advantage that no dragging torque is produced in the case of phase short-circuits, [15]; nevertheless, some key figures such as power-to-weight and power-to-size ratios, and efficiency, which are relevant for aircraft actuators, could be lower in principle without accurate design, and they need to be carefully evaluated for the given application, [16].

In the recent past, the authors proposed multi-phase PM machines with modular structure for aircraft applications, including an actuator designed for the deployment of the wing's flaps, [17].

M. Tursini, M. Villani, and G. Fabri are with the Department of Industrial and Information Engineering and Economy, University of L'Aquila, I-67100 L'Aquila, Italy.

L. Di Leonardo is with R13 technology srl., I-67100 L'Aquila, Italy. (e-mails: marco.tursini@ing.univaq.it; marco.villani@univaq.it; giuseppe.fabri@univaq.it; dileonardolino@gmail.com).

The block scheme of the flap-actuator concerned is shown in Fig. 1. It is based on a rotating electric motor with a ball-screw device integrated into the rotor body, which turns the rotational motion in a linear movement. The developed prototype refers to a medium size aircraft (120-180 passengers). The specifications of an electrical motor matching to such ratings are shown in Table I, in which the stack length and outer stator diameter have been fixed for the encumbrance limits and the maximum speed depends on the transmission ratio of the ball-screw device and the linear speed requested by the flap panel.

In this paper a five-phase fault-tolerant SR machine developed for the same flap actuator is concerned, and design details, prototyping issues and performance are presented. The work completes the study illustrated in [18] and will enable, in the near future, a comparative evaluation between PM and SR machines in order to identify the better solution for such specific application.

The paper is organized as follows: preliminary design issues and sizing equations of the SR motor are resumed in Section II; torque production principles and related feeding strategy are presented in Section III; the design refinement by means of finite element analysis is discussed Section IV; performance analysis and optimization of the feeding strategy are shown in Section III; the multi-phase fault tolerant control scheme is presented in Section VI; finally, experimental verification of the SR motor-drive prototype is reported in Section VII.

TABLE I
SPECIFICATIONS OF AN ELECTRICAL MOTOR FOR FLAP ACTUATOR

DC voltage supply (max)	V	250
Rated torque in the healthy mode operation	Nm	12.0 @ 600 rpm
Weight	kg	<4.0
Stack length	mm	60
Outer stator diameter	mm	110
Cooling system		natural air
Torque with one phase open	Nm	12.0 @ 600 rpm
Torque with two phases open	Nm	12.0 @ 400 rpm

II. SWITCHED-RELUCTANCE MOTOR DESIGN

The SR motor is a type of reluctance motor, doubly salient with phase coils mounted around diametrically opposite stator poles. There are no windings or permanent magnets on the rotor, which is basically a piece of steel (and laminations) shaped to form salient poles. The stator has concentrated coils on $N_s = 2mq$ stator poles where m is the number of phases and q is the number of the stator poles pairs per phase, while the rotor has N_r poles.

The cross section of the SR motor presented in this paper is shown in Fig. 2. According to the multiphase constraint of the flap actuator application it has $m = 5$ phases, whereby a solution with $N_s = 10$ stator poles and $N_r = 8$ rotor poles has been chosen: the concentrated windings on the diametrically opposite poles are connected in series.

The torque comes from the tendency of the rotor poles to align with the excited stator poles; it follows that to achieve smooth torque generation the phase feeding must be switched according to the rotor position.

The structure here considered foresees two adjacent phases conducting simultaneously according to the winding signs depicted in the cross-section scheme: such feeding strategy and the related commutation logic will be discussed in the next Section III.

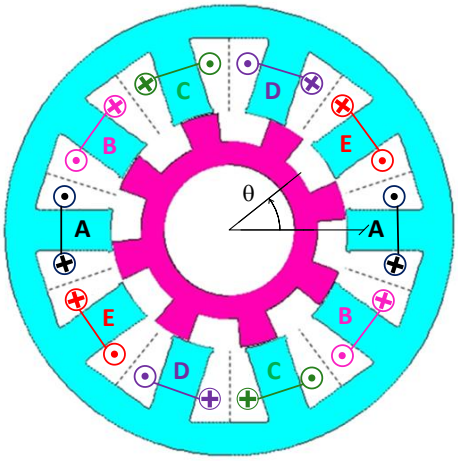

Fig. 2. Cross-section and winding distribution of the five-phase 10/8 SR motor.

The preliminary performance analysis of the SR motor requires defining the dimensions for stator and rotor shapes, stator windings, pole numbers, and pole arcs.

An approximate sizing of the SR motor is obtainable by using the output power equation (1), which relates bore diameter and length, speed, and magnetic and electric loadings as follows, [2]:

$$P_o = \left(\frac{\pi^2}{120}\right) a\gamma\,\eta D^2 L\, B\Delta n_s \qquad (1)$$

where the parameters a and γ can be computed as:

$$a = \left(1 - \frac{1}{k_1 k_2}\right) \qquad (2)$$

$$\gamma = \frac{\alpha_c N_{ph} N_r}{360} \qquad (3)$$

where:

- k_1 is the ratio between the aligned saturated inductance per phase and the aligned unsaturated inductance per phase;
- k_2 is the ratio between the aligned unsaturated inductance per phase and the unaligned inductance per phase;
- α_c is the current conducting angle for each rising inductance profile.

As one can see, the output power is proportional to the product of specific electric and magnetic loadings and bore volume. Once the motor ratings are defined and loadings are fixed, the machine dimensions can be computed through an iterative process of steady-state performance calculations. The design process can start by imposing γ equal one and a reasonable value to the constant a. In general, at the rated operating point, this value is in the range between $0.65 \div 0.75$. The specific electric loading Δ is given by:

$$\Delta = \frac{N'_{ph} 2 N_t I}{\pi D} \qquad (4)$$

and its value can be selected in a range between $20000 \div 90000$ A/m.

Then, the ratio between the stack length L and the bore diameter D is fixed, which depends on the specific application and it is in the range between $0.4 \div 2.0$.

The number of turns per phase N_t can be evaluated using equation (4), and the wire size is chosen according to the maximum available slot fill factor. The knowledge of the space available for the stator winding enables the calculation of the height of the stator pole.

Finally, the other motor dimensions in terms of stator and rotor pole arcs, stator and rotor back iron thicknesses, stator and rotor pole height, air-gap length, can be evaluated by using typical relationships proposed by several authors, e.g. [2], [1].

By using the sizing procedure resumed above, a preliminary design of the SR motor has been identified whose main dimensions are shown in Table II. The stator and rotor lamination is a traditional *800-50* electrical steel, *0.50* mm thickness. Moreover, a conventional temperature of *75°C* has been imposed for the stator winding.

TABLE II
SR MOTOR: PRELIMINARY DESIGN

Number of stator poles		10
Number of rotor poles		8
Number of phases		5
Stack length	mm	60
Outer stator diameter	mm	110
Inner stator diameter	mm	64
Turns per phase		180
Wire size	mm^2	0.70
Air-gap length	mm	0.35
Lamination material		800-50
Phase resistance (75°C)	Ω	1.13
Average torque @ 600 rpm	Nm	12.5
Phase current	A	30
Torque constant k_T	Nm/A	0.42

III. FEEDING STRATEGY AND TORQUE PRODUCTION

The proposed SR motor is designed to operate with two adjacent phase conducting simultaneously in proper angular sector of rotor position ("two-phase feeding"), in order to get maximum torque capability.

The feeding sector of each phase can be defined, under some simplifying assumptions, by considering the profile of the phase inductance as a function of the rotor angular position, [19].

In fact, the electromagnetic torque produced by the motor can be obtained through the general relation, [20]:

$$T = \frac{dW_c(\underline{i}, \theta)}{d\theta} \qquad (5)$$

where W_c is the magnetic co-energy stored in the set of coupled phase windings, $\underline{i}$ is a functional notation for the winding currents, θ is the rotor electrical position, and the mentioned magnetic co-energy is defined as:

$$W_c(\underline{i}, \theta) = \int \underline{\lambda}(\theta, \underline{i}) d\underline{i} \qquad (6)$$

being $\underline{\lambda}$ the functional notation of the flux linkages of the coupled windings.

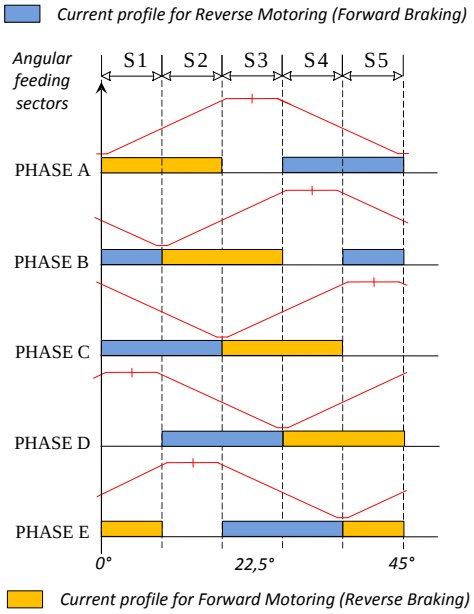

Fig. 3. 2-phases-on feeding strategy of the SR motor vs. ideal profile of phase inductances.

In case of linearity of the magnetic circuit and considering only two phases x and y in conduction, the torque expression becomes:

$$T = \frac{1}{2} i_x^2 \frac{dL_{xx}(\theta)}{d\theta} + i_x i_y \frac{dL_{xy}(\theta)}{d\theta} + \frac{1}{2} i_y^2 \frac{dL_{yy}(\theta)}{d\theta} \qquad (7)$$

where L_{xx}, L_{yy} are the self-inductances of phases x and y and L_{xy} is the mutual inductance between them, all functions of the rotor position.

If the mutual coupling is neglected, the torque can be seen as the independent contribution of each phase (by the square of its current) as acting alone, where the amount and sign depends on the shape of the phase sel-inductance by its derivative.

Fig. 3 shows the phase feeding pattern of the considered SR motor, assuming an ideal profile of the phase self-inductance calculated from the geometry of the machine and schematically reported in the same figure, [2].

In a 10/8 stator/rotor poles machine, the inductance profile on each stator pole pair is periodic of 45 degrees, while each pole is displaced of 9 degrees from the other. In this figure (such as in the following analyses) the rotor position is measured from the axis of the phase *A* stator pole to the center of the base between two arbitrary (adjacent) rotor teeth (see Fig. 2). Then the zero of the rotor position corresponds to the so-called "unaligned" position (minimum inductance) of the phase *A*.

Feasible phase current profiles for motoring and braking torque generation are also reported in the figure considering that the sign of the torque contribution is imposed by the derivative of the inductance vs. rotor position.

Therefore five angular sectors (S1 to S5) can be defined

from the inductance profiles and the feeding logic and commutation angles of each phase can be recognized.

Anyway, it should be recalled that the SR motor is generally a highly saturated electromagnetic structure with strongly non-linear flux-current relations; moreover the coupling between the phases fed simultaneously must be considered. How to account for these matters is the argument of the next sections.

IV. Finite Element Analysis and Design Refinement

The design of the SR motor has been completed by an accurate calculation of the flux linkages and torque production vs. feeding currents and rotor position. This analysis has been carried out by the Finite Element (FE) method that is a powerful analytical tool to analyze complex and non-linear electromagnetic structure like the SR motor, [21].

A versatile two-dimensional (2D) FE model has been developed with variable motor dimensions in order to enable the design optimization. For this reason, a "parametric" model of the machine has been carried out which uses a limited number of independent parameters to define the geometry of the motor itself. The mesh has been accurately refined in the air-gap and in the regions where the flux density was expected to be high.

Since the proposed 10/8 SR motor is designed to work with two phases conducting simultaneously, the evaluation of motor performance has been carried out assuming the 2-phases on feeding strategy of Fig. 3. A static analysis is performed over the rotor angle variation, i.e. the phase currents are supposed to have ideal square-wave shapes with constant maximum value (transient phenomena are neglected).

The preliminary design of the motor has been gradually refined combining the FE model with an optimization algorithm belonging to the class of Controlled Random Search algorithms, [22]. The optimization procedure uses the information obtained by the FE program to iteratively update the set of motor parameters and try to identify an "optimal" motor by making a trade-off between the different parameters of the machine.

The chosen design variables include the geometric dimensions (Fig. 4), the number of turns per phase and the wire size. The stator pole tapering has significant impact on shaping the electromagnetic torque and self-inductances, whereas the rotor pole tapering is of no consequence, but this solution affects the slot fill factor and the winding insertion. For these reasons, in the proposed design, the stator and rotor poles do not present any taper.

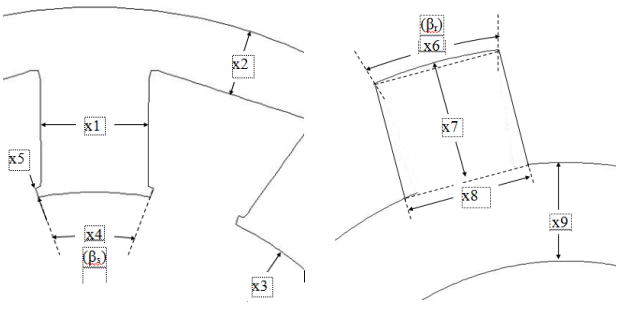

Fig. 4. Design variables of the Switched Reluctance motor: stator (left) and rotor (right) details.

The aim of the optimization was to maximize the torque constant in the healthy mode operation and satisfy the following constraints:

- slot fill factor ≤ 0.45;
- flux density in the stator teeth ≤ 1.8 T;
- flux density in the stator yoke ≤ 1.7 T;
- average torque in the healthy mode operation > 12 Nm.

The results of the optimization process are presented in Table III, which includes some of the key machine dimensions and the torque-to-current performance at *600 rpm* in the healthy mode and faulty mode operations. One notices that in the healthy operation, the torque-to-current ratio is higher than in the preliminary design (Table II).

In faulty modes a new value for the current in the healthy phases has been imposed (see Table III), in order to satisfy the degraded operating modes.

TABLE III
SR MOTOR: OPTIMIZED DESIGN

Stack length	mm	60
Outer stator diameter	mm	110
Inner stator diameter	mm	70
Shaft diameter	mm	40
Rotor to stator pole arc ratio (β_r/β_s)		0.92
Stator pole arc to pole pitch ratio		0.54
Rotor pole arc to pole pitch ratio		0.40
Turns per phase		164
Wire size	mm^2	0.50
Slot fill factor		0.45
Phase resistance (75°C)	Ω	1.17
Healthy mode operation:		
Average torque @ 600 rpm	Nm	14.0
Phase current	A	25
k_T	Nm/A	0.56
Faulty mode: one phase open:		
Average torque @ 600 rpm	Nm	13.3
Phase current	A	30
Faulty mode: two phases open:		
Average torque @ 600 rpm	Nm	13.0
Phase current	A	45

Finally, flux distribution and inductance computation are presented as meaningful outputs of the FE design process:

- Fig. 5 shows the flux lines distribution computed by the FE analyses in the case of the feeding of two contiguous phases, which is the normal operation in healthy conditions. One notices that the flux lines close themselves for the most part inside the contiguous poles belonging to the fed phases, giving the characteristics "short path" feature to the flux distribution.
- Fig. 6 shows the flux lines distribution when just one phase is fed, a type of operation which occurs in case of an open phase fault, during two consecutive angular sectors. In this case the flux lines close themselves for the most part inside the opposite poles belonging to the unique fed phase, resulting in a "long path" flux

distribution, strongly different from the previous one.

- Fig. 7 shows the phase self-inductance versus rotor position calculated by FE analysis for different current values: the kind of profile corresponds to that assumed to set-up the basic feeding strategy of the SR motor (compare with Fig. 3).

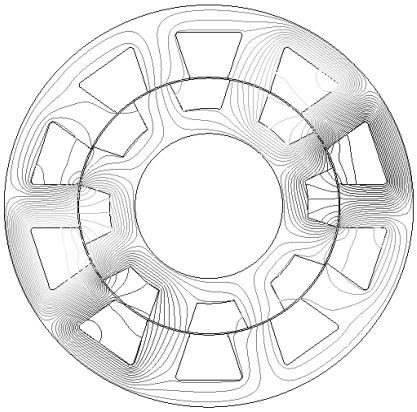

Fig. 5. Two-phase feeding: static flux line distribution (phases *A* and *E* are fed in feeding sector S1).

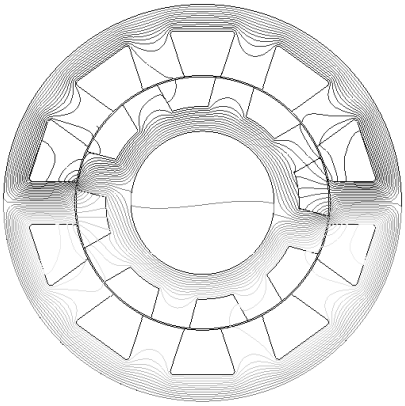

Fig. 6. One-phase feeding: static flux line distribution (phase *A* is fed).

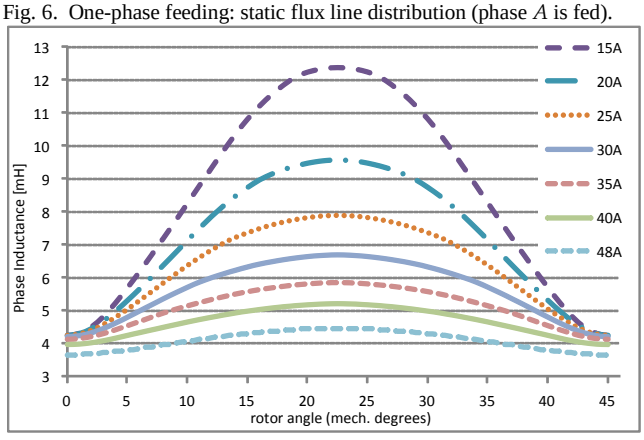

Fig. 7. Optimized design: phase inductance vs. rotor position at different values of phase currents.

V. Performance Analysis and Optimization of the Feeding Strategy

The proposed motor is designed to generate the torque when two adjacent phases are fed simultaneously. Moreover the motor is designed to possess fault-tolerance capabilities in case of the loss of one or two phases.

It happens that in faulty modes the motor work with only one phase fed in some angular sectors. For this instance the static FE analysis study has been performed for both the one-phase and two-phase feeding cases to predict the performance of the machine in all the possible conditions.

One-phase feeding

In this case the SR motor behaves as a "long path" flux machine (see Fig. 6 for flux lines distribution); the flux linkage vs. rotor angle computed by the FE analysis are shown in Fig. 8 for different values of current (phase *A* is considered). The effect of saturation at high current levels is clearly visible around the alignment of stator pole and rotor tooth ("aligned" position, 22.5 mech. degrees in case of phase *A*).

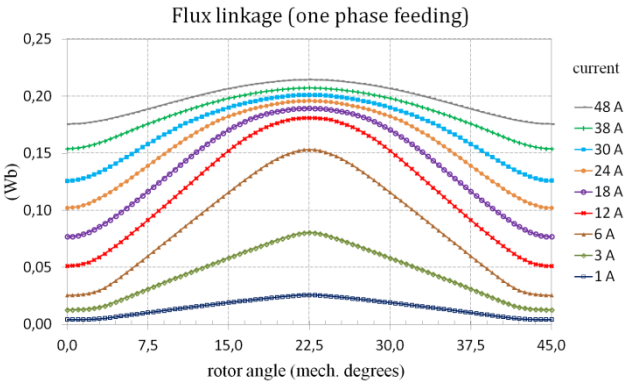

Fig. 8. Flux linking the phase *A* (when only this phase is fed).

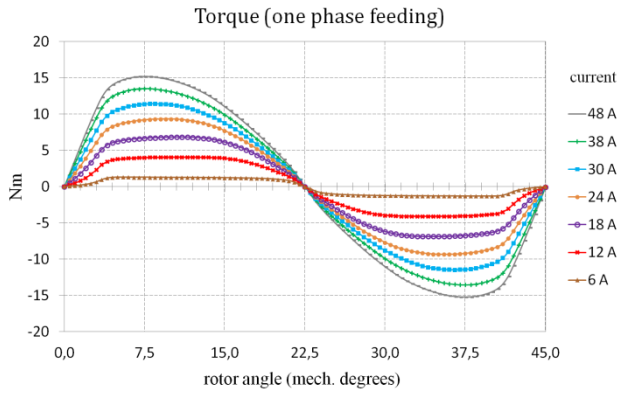

Fig. 9. Torque produced by feeding the phase *A* only.

Fig. 9 shows the torque as a function of the rotor position when the phase *A* is fed. The same simulation has been done for different current values, up to current ratings adopted in faulty mode operations (48A). The torque is positive for rotor position ranging from zero to the "aligned" position, while it is negative from that position to the end of the pole period. The effect of saturation is the shift of the maximum torque position toward the "unaligned" position, and this suggests an adaptation of the commutation angles as function of the current values at least for high loading.

Two-phase feeding

In this case the SR motor behaves as a "short path" flux machine (see Fig. 5 for flux lines distribution); the flux linkages vs. rotor angle computed by the FE analysis are shown in Fig. 10 and Fig. 11 for the phases *A* and *E* respectively, for different values of the phase current (the same current value in the two phases is considered). The effect of saturation is still evident; moreover there is a certain distortion caused by the magnetic coupling if compared to the case of one-phase feeding.

The torque generated by the two phases is shown in Fig. 12. As expected, it is greater than in the one-phase feeding at same current, but due to saturation it grows less than linearly. The zeros and (roughly) maximum values are shifted of half the contiguous poles displacement (4.5 degrees) as obvious; moreover, one still observes an increased distortion of the profiles.

Considering that the feeding state of phases *A* and *E* corresponds to that of the angular sector S1 (see Fig. 3), the (static) torque produced by the 2-phases-on feeding strategy can be obtained by replicating the torque produced in S1 (see the window in Fig. 12) over the remaining sectors of the pole period.

Hence, the static total torque plots obtained for different current values are reported in Fig. 13. It can be noticed that the torque profiles obtained at current values greater than the rated one exhibit increasing torque ripple vs. (mean) produced torque.

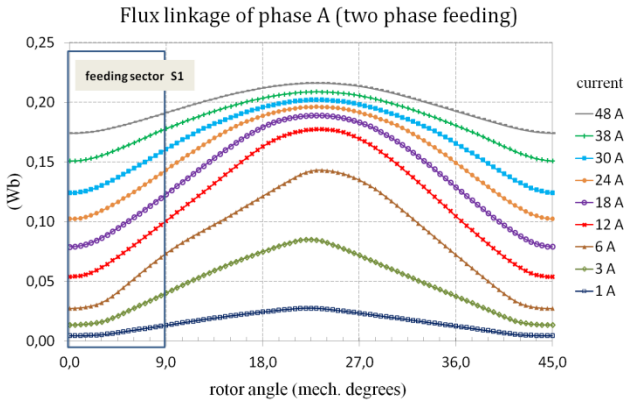

Fig. 10. Flux linkage of phase *A* by assuming the two-phase feeding of phases *A* and *E*.

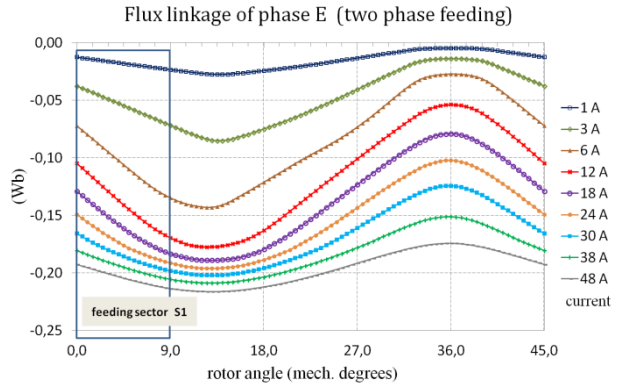

Fig. 11. Flux linkage of phase *E* by assuming the two-phase feeding of phases *A* and *E*.

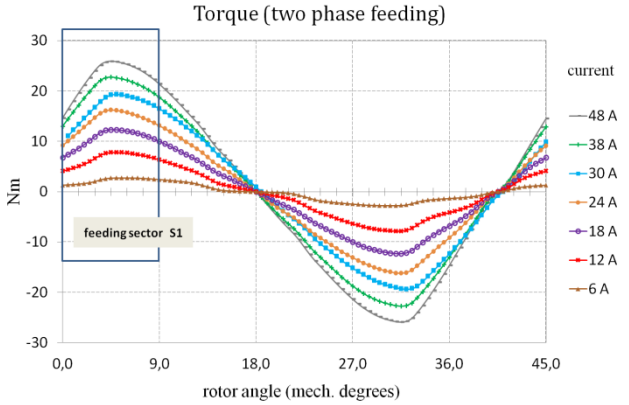

Fig. 12. Torque produced by the two-phase feeding operation of phases *A* and *E*.

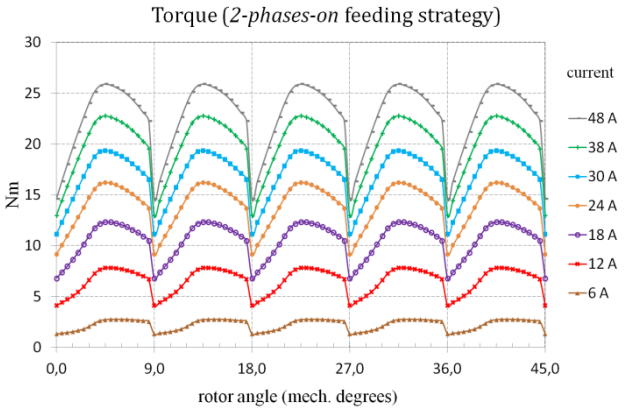

Fig. 13. **Static** torque produced by the "2-phases-on" feeding strategy.

Although the torque ripple is considered a secondary problem in the flap actuation by EMAs (and the aircraft manufacturers do not provide specific requirements in the ongoing research projects) it is evident that it cannot be neglected. Hence, its minimization is discussed below.

To improve the static torque ripple a commutation angle can be adopted (Fig. 14) with possible benefits also in term of mean value of the produced torque, [23].

The total static torque produced by the SR motor through optimization of the commutation angles is reported in Fig. 15. The amount of the compensation can be evaluated by comparison with Fig. 13. It is basically a delay angle which varies depending on the current value in a range between 1.5 and 3 degrees (maximum the 30% of the feeding sector). The advantage achieved in terms of torque ripple in comparison with the "base" solution (commutation angles nil) is detailed in Fig. 16. One can notice that the reduction of the ripple is relevant at all the current ratings, meaning that such solution is adoptable also when the motor would work in saturated conditions. On the contrary, the increase of the mean torque appears negligible, Fig. 17.

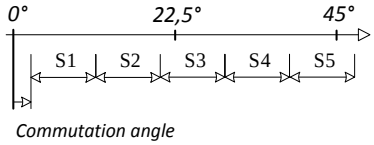

Fig. 14. Definition of the commutation angle.

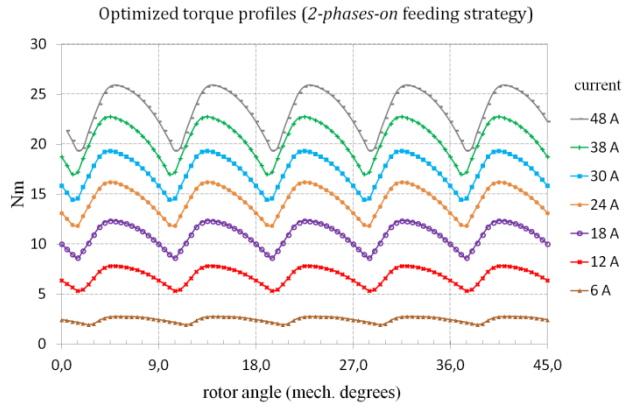

Fig. 15. **Static** torque produced by the "2-phases-on" feeding strategy with optimization of the commutation angle.

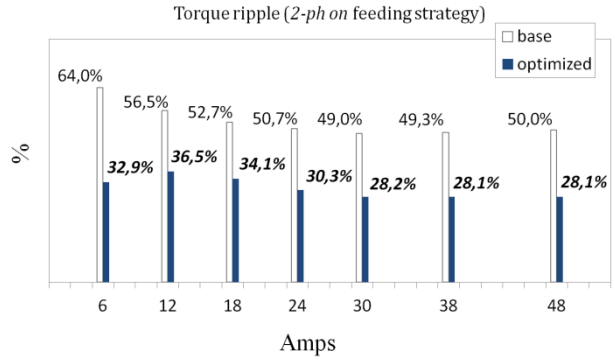

Fig. 16. **Static** torque ripple produced by the "2-phases-on" feeding strategy.

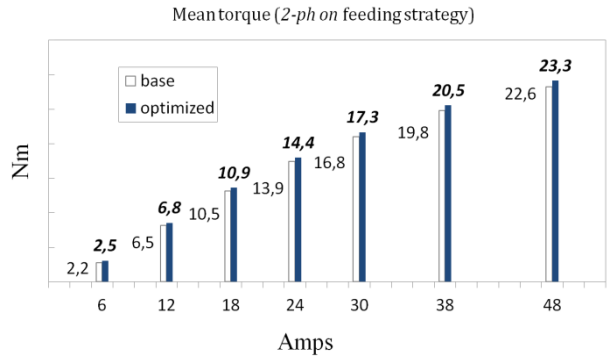

Fig. 17. Average **static** torque produced by the "2-phases-on" feeding strategy.

VI. Fault Tolerant Control Scheme

The control scheme adopted for the SR motor is presented in Fig. 18. According to the fault-tolerance principles, modular architecture has been adopted in current control, with five independent control loops which regulate each phase current. In each current loop the error between the reference and the measured current is regulated by means of Proportional-Integral (PI) regulator and the correction is applied to the single-phase voltage-source inverter through Pulse Width Modulation (PWM).

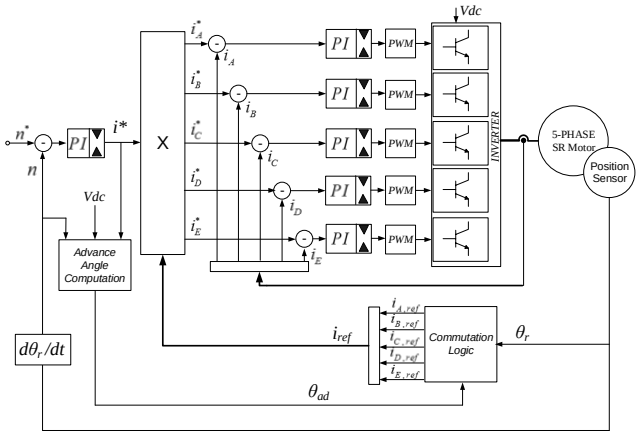

Fig. 18. Control scheme of the five-phase SR machine.

An external PI speed control loop regulates the speed by comparison with the respective reference, and it generates the torque requirement in term of reference amplitude for the inner current loop. Commutation logic is provided which implements the 2-phases-on feeding strategy: it generates the square wave shapes of the current references from the measure of the rotor angle.

A mechanism to introduce an advance angle between the measure of the rotor position and the generation of the commutation logic (i.e. the feeding sectors) is included. It permits to compensate for the rising time of the current and provide acceptable torque ripple/noise also at high speed, [19]. Such a feature gives also the opportunity to implement the optimization angle discussed in the Section V.

It should be noted that such a simple control scheme automatically reacts in case of fault of one phase even without any diagnostic mechanism.

The fault is recognized by a speed error and corrected by the current control loop that increases the current (torque) commands of the healthy phases to recover the desired speed. Of course a proper detection of the fault gives advantages in term of speed and quality of the response to the fault, but it is not strictly needed in terms of reliability of the control system.

VII. Prototype and Experimental Results

Starting from the optimized design a prototype of the 10/8 SR motor has been manufactured and tested: Fig. 19 shows a view of the motor with the embedded screw for flap mechanics actuation.

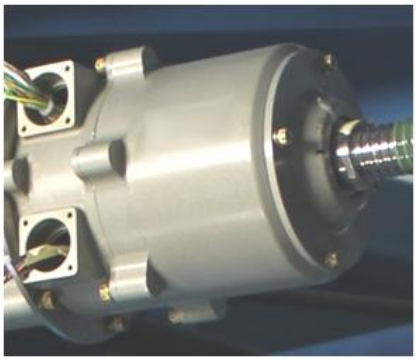

Fig. 19. Prototype of the SR motor assembled in the EMA.

To perform the tests of the machine a multiphase power electronic development platform has been used, Fig. 20. The platform features up to six independent feeding modules each of which integrating a single phase IGBT inverter and current sensor. Power electronics is managed by a TMS320F2808 Digital Signal Processor (DSP) that executes the mentioned control algorithm at about 15 kHz.

Redundant Hall Effect commutation sensors and incremental encoders, embedded in the EMA, are used to evaluate the feeding angular sectors and continuous position and speed signals, respectively.

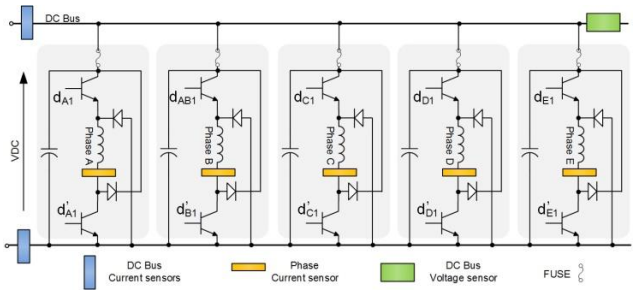

Fig. 20. Modular architecture of the SR multiphase power converter.

Experimental results are shown hereafter. They are achieved by a real-time data acquisition tool working at PWM rate. It is based on a 4-channels-Digital-to-Analog Converter (DAC) which directly sends data signals computed by the drive controller to an oscilloscope.

For a better understanding of the waveforms reported in the tracks let consider some differences between the conventions assumed in the implementation and those considered till now in the paper:

- the zero of the rotor position is assumed at the "aligned" position because an alignment procedure is used to initialize the measure of the incremental encoder;
- some phase currents are plotted with reverse sign in order to avoid superposition of tracks.

Due to limitations of the power converter it was not possible to test the prototype at rated speed and torque conditions, nevertheless meaningful results are achieved both in healthy and faulty mode conditions.

Figures 21 and 22 refer to the healthy mode operation of the machine at constant load-torque and speed:

- Fig. 21 shows the current waveforms of two adjacent phases along with the electrical position and the feeding sector, when the machine is operated at 300 rpm, 8 Nm load torque. One can notice an advance angle of something less than 4.5 degrees used in the computation of the feeding sectors: such a value corresponds to phase the sectors with the ideal shape of the phase inductance considered in theory, plus a small commutation angle. In fact, the currents, are practically unaffected by rising delays at this speed (about half of the rated one) and an actual advance is unnecessary.
- Fig. 22 reports the motor speed and currents in the same torque-speed conditions. One can see how the torque ripple of the motor affects the speed due to the low inertia of the motor.

Figures 23 and 24 refer to the faulty mode operation in the same torque/speed conditions:

- Fig. 23 shows the response in case one phase is suddenly opened. After the fault occurrence, the lack of motor torque depresses the speed slightly and the controller reacts so to increase the amplitude of the (healthy) phase currents. Such an increment is really moderate and, despite the increment of the torque ripple, the operation is maintained at preset speed and load conditions.
- Fig. 24 shows the worst case when two adjacent phases are suddenly and simultaneously opened. In this case the current in the healthy phases increases its value by a more relevant factor, about 1.5. The transient behavior after the fault occurrence is similar to that of the previous case, but the speed fluctuations are larger, due to the presence of higher torque ripples. The operation is maintained at given speed set-point and load, but with high noise and vibration in the rotor. This severe condition requires a proper sizing of both the motor and the coupling mechanics, so that the flap-actuator can reach the target position even in case of fault.

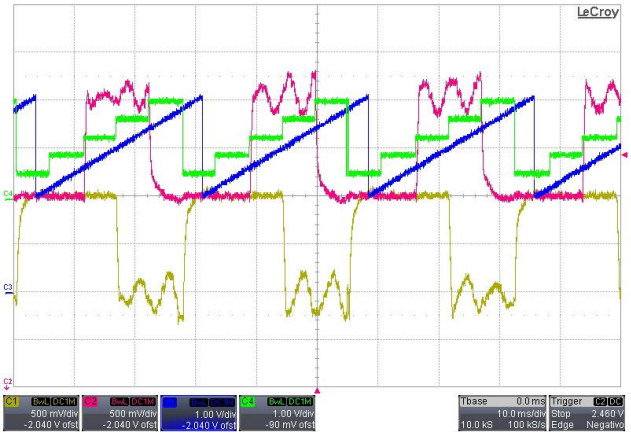

Fig. 21. Healthy mode operation @ 300 rpm, 8 Nm:

Phase–*A* and Phase–*E* measured currents (yellow, red), commutation sector (green), electrical position (blue); current is scaled to 7.5A/div.

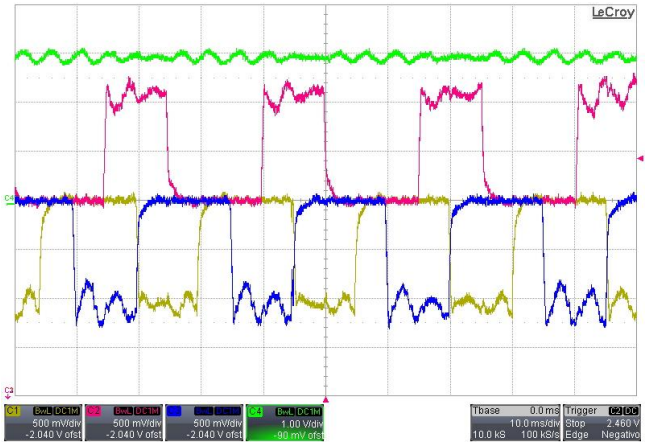

Fig. 22. Healthy mode operation @ 300 rpm, 8 Nm:

Phase–*A*, Phase–*E*, and Phase-*D* measured currents (yellow, red, blue); motor speed (green); current is scaled to 7.5A/div.

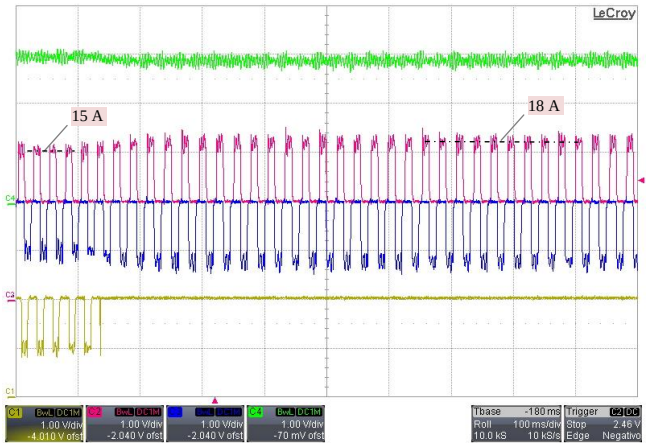

Fig. 23. Faulty mode operation: one phase open fault in phase A @ 300 rpm, 8 Nm:

Measured current of phase *A* (yellow), *B* (red), and *C* (blue); measured rotor speed (green); current is scaled to 15A/div, time 100ms/div.

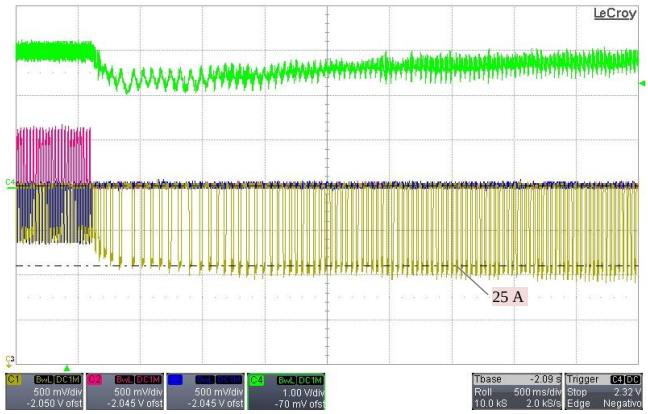

Fig. 24. Faulty mode operation: phase open fault in phases A and B @ 300 rpm, 8 Nm:

Measured current of phase *A* (yellow), *B* (red), and *C* (blue); measured rotor speed (green); current is scaled to 15A/div, time 100ms/div.

Finally, for the sake of comparison, a FE analysis has been carried out by imposing the same maximum currents of the experimental tests in the healthy mode (15 A) and faulty mode operation with one open phase (18 A) and two open phases (25 A), The static torque profiles are shown in Fig. 25 and Fig. 26, the average torque values obtained in these conditions are about 8 Nm which corresponds to the load torque imposed by an hysteresis brake dynamometer in the experimental tests. The torque ripple is 36.8% for the healthy operation.

In case of one or two-phase open, the figures points out a strong torque ripple of 119% and 183% respectively, but also in these severe conditions the experiments demonstrate that the SR motor is able to run and guarantee a safe movement of the flap actuator, such as to ensure the aircraft's stability in the final application.

VIII. Conclusions

A five-phase Switched Reluctance motor has been designed for the flap actuation of medium size aircrafts, and thereafter a prototype has been manufactured and tested. According to the application requirements, the motor has been build to satisfy the load/speed specifications also in case of operation with one or two phases open (faulty modes).

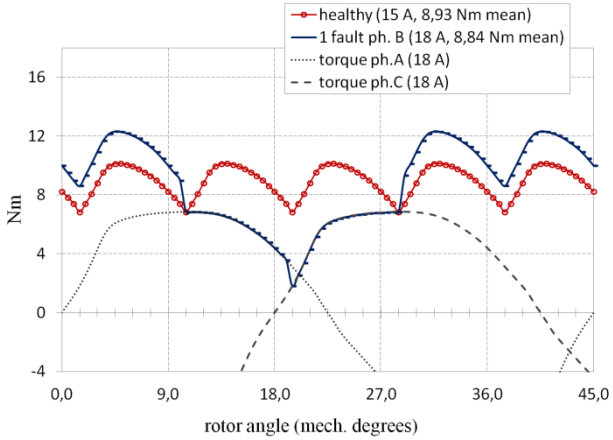

Fig. 25. Static torque vs. rotor position in healthy and faulty operation (one open phase) @ experimental current ratings.

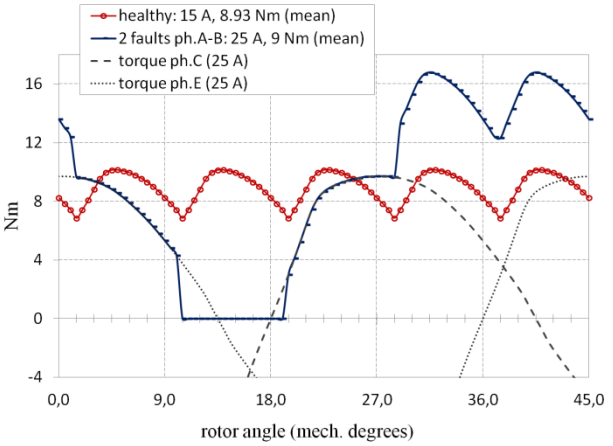

Fig. 26. Static torque vs. rotor position in healthy and faulty operation (two open phases) @ experimental current ratings.

The test results confirm the performance analysis computed by Finite Element model and show that the machine is able to operate in severe faulty mode conditions, although the limitations of the power electronics allowed to test the prototype at only 1/3 of the rated power. Future work will concentrate on the comparison of the SR motor performance with those of a PM machine developed by the authors within the same research project.

Acknowledgements

The project has been developed at the Department of Industrial & Information Engineering and Economy of the University of L'Aquila (Italy) on behalf of Umbra Cuscinetti S.p.A. (Italy) as an R&D project based on an EADS SCD.

Authors would like to thank Luca Castellini, general manager of Umbra Cuscinetti EMA Research Center, for the support in the project's development.

References

[1] B. Amin, Variable Reluctance Machines, Jouve, Paris, 2003.

[2] R. Krishnan, Switched Reluctance Motor Drive, CRC Press, New York, 2001.

[3] T. Nonaka, Y. Nakazawa, K. Ohyama, H. Fujii, H. Uehara, Y. Hyakutake, Inverter improving motor efficiency of switched

reluctance motor for electric vehicle, European Power Electronics Conference, EPE (2013), France, pp. 1-8.

[4] H. Hannoun, M. Hilairet, C. Marchand, Design of an SRM Speed Control Strategy for a Wide Range of Operating Speeds, IEEE Trans. on Industrial Electronics (2010), pp. 2911-2921.

[5] Z. Yueying, W. Dafang, Z. Guifan, Y. Dongyu, W. Yu, Research progress of switched reluctance motor drive system, Int. Conf. on Mechatronics and Automation, ICMA (2009), Changchun, China.

[6] R. Krishnan, Whither motor drives: A case study in switched reluctance motor drives, Int. Conf. on Electrical Machines and Systems, ICEMS (2007), Seoul, South Korea.

[7] M.D. Hennen, M. Niessen, C. Heyers, H.J. Brauer, R.W. De Doncker, Development and Control of an Integrated and Distributed Inverter for a Fault Tolerant Five-Phase Switched Reluctance Traction Drive, IEEE Trans. on Power Electronics, pp. 547-554.

[8] P. Asadi, M. Ehsani, B. Fahimi, Design and control characte-rization of switched reluctance generator for maximum output power, Applied Power Electronics Conf. and Exposition, APEC (2006), Dallas, USA.

[9] A. Radun, Generating with the switched reluctance motor, Proc. of Applied Power Electronics Conf. and Exposition, APEC (1994), vol.1, pp. 41-47.

[10] C. Xiaoyuan, D Zhiquan, P. Jingjing, Li Xiangsheng, Comparison of two different fault-tolerant switched reluctance machines for fuel pump drive in aircraft, Int. Power Electronics and Motion Control Conf., IPEMC (2009), Wuhan, China, pp. 2086-2090.

[11] A. Schramm, D. Gerling, Research on the suitability of Switched Reluctance machines and Permanent Magnet machines for specific aerospace applications demanding fault tolerance, Int. Symp. on Power Electronics, Electrical Drives, Automation and Motion, SPEEDAM (2006), Taormina, Italy.

[12] L. Kaiyuan, A new fault-tolerant switched reluctance motor with reliable fault detection capability, Int. Conf. on Electrical Machines and Systems, ICEMS (2014), Hangzhou, China, pp. 188-1886.

[13] A. Garcia, J. Cusido, J.A. Rosero, J.A. Ortega,, L. Romeral, Reliable electro-mechanical actuators in aircraft, IEEE Aerospace and Electronic Systems Magazine (2008), vol. 23, pp. 19-25.

[14] M. Villani, M. Tursini, G. Fabri, L. Castellini, Multi-Phase Fault Tolerant Drives for Aircraft Applications, Int. Conf. on Electrical Systems for Aircraft, Railway and Ship Propulsion, ESARS (2010), Bologna, Italy.

[15] A.G. Jack, B.C. Mecrow, J.A. Haylock, A Comparative Study of Permanent Magnet and Switched Reluctance Motors for High-Performance Fault-Tolerant Applications, IEEE Trans. on Industry Applications (1996), vol. 32, pp. 889 - 895.

[16] R. Krishnan, A.S. Bharadwaj, A comparative study of various motor drive systems for aircraft applications, IEEE Industry Appl. Society Annual Meeting (1991), vol.1, pp. 252-258.

[17] M. Villani, M. Tursini, G. Fabri, L. Castellini, High Reliability Permanent Magnet Brushless Motor Drive for Aircraft Application, IEEE Trans. on Industrial Electronics (2012), vol. 59, pp. 2073-2081.

[18] M. Villani, M. Tursini, G. Fabri, L. Di Leonardo, A switched-reluctance motor for aerospace application, Int. Conference on Electrical Machines, ICEM (2014), pp. 2073 -2079.

[19] B.K. Bose, T.J.E. Miller, P.M. Szczesny, W.H. Bicknell, Micro-computer Control of Switched Reluctance Motor, IEEE Trans. on Industry Applications, 1986, vol. 22, pp. 708-715.

[20] P.C. Krause, O. Wasynczuk, Electromechanical Motion Devices, McGraw-Hill, New York, 1989.

[21] H. Torkaman, E. Afjei, P. Yadegari, Static, Dynamic, and Mixed Eccentricity Faults Diagnosis in Switched Reluctance Motors Using Transient Finite Element Method and Experiments, IEEE Trans. on Magnetics (2012), pp 2254-2264.

[22] F. Parasiliti, M. Villani, S. Lucidi, F. Rinaldi, Finite Element Based Multi-Objective Design Optimization Procedure of Interior Permanent Magnet Synchronous Motors for Wide Constant-Power Region Operation, IEEE Trans. on Industrial Electronics (2012), vol. 59, n.6, pp. 2503-2514.

[23] C. Mademlis, I. Kioskeridis, Performance optimization in switched reluctance motor drives with online commutation angle control, IEEE Trans. on Energy Conversion, (2003), vol. 18, pp. 448-457.